ORIGINAL PAPER - PRODUCTION ENGINEERING

Modeling hydraulic fractures in finite difference simulators using amalgam local grid refinement (LGR)

Reda Abdel Azim · Sherif S. Abdelmoneim

Abstract Hydraulic fracturing allows numerous, otherwise unproductive, low-permeability hydrocarbon formations to be produced. The interactions between the fractures and the heterogeneous reservoir rock, however, are quite complex, which makes it quite difficult to model production from hydraulically fractured systems. Various techniques have been applied in the simulation of hydraulically fractured wells using finite difference simulators; most of these techniques are limited by the grid dimensions and computing time and hardware restrictions. Most of the current analytical techniques assume a single rectangular shaped fracture in a single-phase homogeneous reservoir, the fracture is limited to the block size and the fracture properties are adjusted using permeability multiplier. The current work demonstrates how to model these systems with a smaller grid block size which allows you to apply sensitivity to the fracture length and model the fracture with enhanced accuracy. It also allows you to study the effect of reservoir heterogeneity on the fractured well performance. It is proposed to apply amalgam LGR technique to decrease the grid size to the dimensions of the hydraulic fracture without dramatically increasing the number of grid blocks which would cause a great increase in the computing time and the model size with no added value. This paper explains how the amalgam LGR is designed and compares between standard LGRs and the proposed design and a case study is presented from an anonymous field in Egypt to illustrate how to use this technique to model the hydraulically fractured well. The simulation model is matched to available production data by changing fracture lengths. Then the model is used to predict future response from the wells. The advantage of this technique is that it allows hydraulically fractured reservoirs to be modeled with less grid size which will lead to more realistic models and more accurate predictions; however, the most useful application of this technique may be in the fracture modeling stage. With this tool, various fracture geometries and scenarios can be tested in the simulator, and the most economic scenarios selected and implemented. This will lead to better fracture placement, and ultimately greater production.

Keywords Hydraulic fracture · Finite difference · Finite element · Amalgam LGR

Abbreviations

LGR	Local grid refinement, it is a widely used expression for the process of dividing one or several grids in the reservoir model into smaller sized grids allowing enhanced grid definition, which is useful for modeling wells or hydraulic fractures and other complex reservoir structures
DOE	Department of Energy, governmental department whose mission is to advance energy technology and promote related innovation in the United States

R. A. Azim (✉)
School of Petroleum Engineering, University of New South Wales, Sydney, Australia
e-mail: reda.abdelazim@student.unsw.edu.au

S. S. Abdelmoneim
ENAP Sipetrol, Cairo, Egypt

مدينة الملك عبدالعزيز
KACST للعلوم والتقنية · Springer

| Tailored pulse fracturing | Employed to control the extent and direction of the produced fractures by the ignition of precise quantities of solid rocket fuel-like proppants in the wellbore to create pressure 'pulse' which creates fractures in a more predictable pattern |
| Foam fracturing | Using foam under high pressure in gas reservoirs. It has the advantage over high-pressure water injection because it does not create as much damage to the formation, and well cleanup operations are less costly |

List of symbols

CO_2, sand fracturing	Increases production by eliminating much of the inhibiting effects of pumped fluids such as plugging by solids, water retention, and chemical interactions
σ_{min}	The minimum horizontal stress (in situ stress)
v	Poisson's ratio
σ_{ob}	Overburden stress
α	Biot's constant
σ_p	Reservoir fluid pressure or pore pressure
σ_{ext}	Tectonic stress
V_p	Average compressional velocity
V_s	Shear velocity
σ_1	Total vertical stress (overburden)
n_x	x-Component of unit normal vector to the boundary
n_y	y-Component of unit normal vector to the boundary
N_p	Pressure shape function
N_u	Displacement shape function
u	Displacement (L, ft)
σ_h	Minimum in situ horizontal stress (m/Lt^2)
σ_H	Maximim in situ horizontal stress (m/Lt^2)
Ω	Domain of the problem
Φ	Porosity

Introduction

Hydraulic fracturing is the process of pumping a fluid into a wellbore at an injection rate that is too high for the formation to accept in a radial flow pattern. As the resistance to flow in the formation increases, the pressure in the wellbore increases to a value that exceeds the breakdown pressure of the formation that is open to the wellbore. Once the formation "breaks-down", a crack or fracture is formed, and the injected fluid begins moving down the fracture.

DOE research has developed several alternative fracturing techniques designed to accomplish specific tasks such as:

- Tailored pulse fracturing
- Foam fracturing
- CO_2, sand fracturing

In general, hydraulic fracture treatments are used to increase the productivity index of a producing well or the injectivity index of an injection well. The productivity index defines the volumes of oil or gas that can be produced at a given pressure differential between the reservoir and the well bore. The injectivity index refers to how much fluid can be injected into an injection well at a given differential pressure.

One of the major problems facing the reservoir engineers in modeling the hydraulic fractures using the finite difference simulators is the wide gap between the grid size of the reservoir model and the fracture dimensions.

The purposes of this paper are to model the flow of the reservoir fluid in hydraulically fractured reservoir using finite difference simulators in a manner that would allow the simulator to mimic the actual fracture geometry without dramatically increasing the number of grid cells and hence increasing the computing requirements and time. This is achieved as shown in the paper by using amalgam LGR to decrease the fractures dimensions to the size and dimensions required to achieve this goal and leave the number of grid cells only slightly affected which makes a minor change in the required computing time and capabilities. This design was tried on an anonymous field in the western dessert in Egypt, and the results were compared with the actual production data which was recorded after the fracture to verify that the model was capable of modeling the actual reservoir performance.

Hydraulic fracture mechanics

The theory of hydraulic fracturing depends on an understanding of crack behavior in a rock mass at depth. Because rock is predominantly a brittle material, most efforts to understand the behavior of crack equilibrium and growth in rocks have relied on elastic, brittle fracture theories.

However, certain aspects, such as poroelastic theory, are unique to porous, permeable underground formations. The
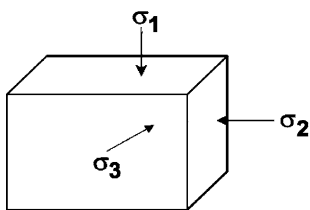
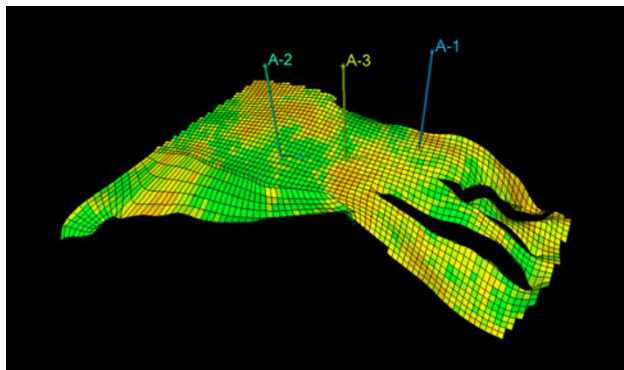Fig. 1 The local stress state at depth for an element of formation

Fig. 2 Overview of the static model

Table 1 Porosity and permeability of the studied field

Formation	Average porosity (ϕ)	Average permeability (k)
Abu-Roash G	0.12–0.15	0.8–1 md

most important parameters are in situ stress, Poisson's ration, and Young's modulus.

In situ stresses

Underground formations are confined and under stress. Figure 1 illustrates the local stress state at depth for an element of formation. The stresses can be divided into three principal stresses. In Fig. 1, σ_1 is the vertical stress, σ_2 is the maximum horizontal stress, while σ_3 is the minimum horizontal stress, where $\sigma_1 > \sigma_2 > \sigma_3$. These stresses are normally compressive and vary in magnitude throughout the reservoir, particularly in the vertical direction (from layer to layer). The magnitude and direction of the principal stresses are important because they control the pressure required to create and propagate a fracture, the shape and vertical extent of the fracture, the direction of the fracture, and the stresses trying to crush and/or embed the propping agent during production.

A hydraulic fracture will propagate perpendicular to the minimum principal stress (σ_3). If the minimum horizontal stress is σ_3 the fracture will be vertical and, we can

compute the minimum horizontal stress profile with depth using the following equation.

$$\sigma_{\text{Min}} \cong \frac{v}{1-v}\left(\sigma_{\text{ob}} - \alpha\sigma_{\text{p}}\right) + \alpha\sigma_{\text{p}} + \alpha_{\text{ext}}$$

Poisson's ratio can be estimated from acoustic log data or from correlations based upon lithology. The overburden stress can be computed using density log data. The reservoir pressure must be measured or estimated. Biot's constant must be less than or equal to 1.0 and typically ranges from 0.5 to 1.0. The first two terms on the right hand side of the equation represent the horizontal stress resulting from the vertical stress and the poroelastic behavior of the formation.

Poroelastic theory can be used to determine the minimum horizontal stress in tectonically relaxed areas (Salz 1977). Poroelastic theories combine the equations of linear elastic stress–strain theory for solids with a term that includes the effects of fluid pressure in the pore space of the reservoir rocks.

The fluid pressure acts equally in all directions as a stress on the formation material. The "effective stress" on the rock grains is computed using linear elastic stress–strain theory. Combining the two sources of stress results in the total stress on the formation, which is the stress that must be exceeded to initiate fracturing. In addition to the in situ or minimum horizontal stress, other rock mechanical properties are important when designing a hydraulic fracture. Poisson's ratio is defined as "the ratio of lateral expansion to longitudinal contraction for a rock under a uniaxial stress condition (Gidley et al. 1989)".

The theory used to compute fracture dimensions is based upon linear elasticity. To apply this theory, the modulus of the formation is an important parameter. Young's modulus is defined as "the ratio of stress to strain for uniaxial stress (Gidley et al. 1989)".

The modulus of a material is a measure of the stiffness of the material. If the modulus is large, the material is stiff. In hydraulic fracturing, a stiff rock will result in more narrow fractures. If the modulus is low, the fractures will be wider. The modulus of a rock will be a function of the lithology, porosity, fluid type, and other variables.

Field case study

Field characterization

We conducted a fracture reservoir simulation study for well A-1 (Appendix 1, Fig 16) over Abu-Roash G reservoir in the field (A), in the western dessert of Egypt.

This field produced light gravity oil (37° API) from Abu-Roash G sand at an average drilled depth of 5,400 ft TVDSS. Only two wells were drilled in the area and had

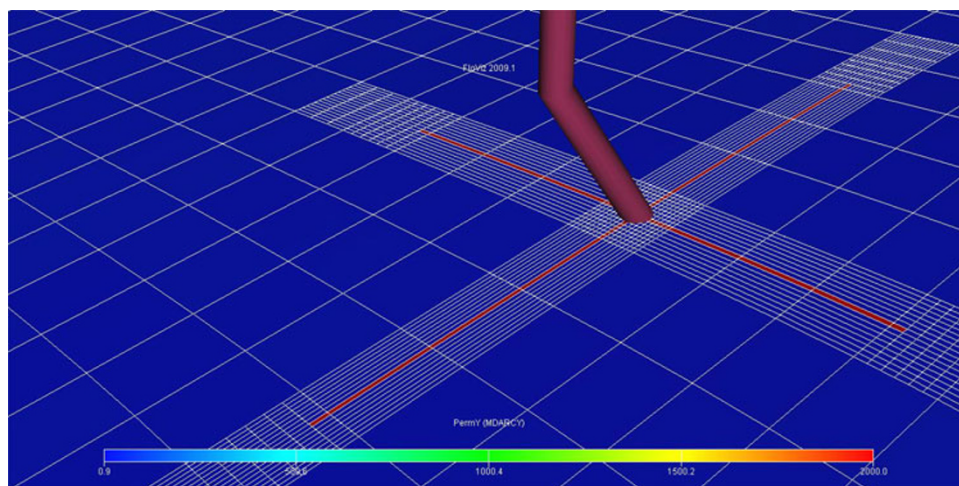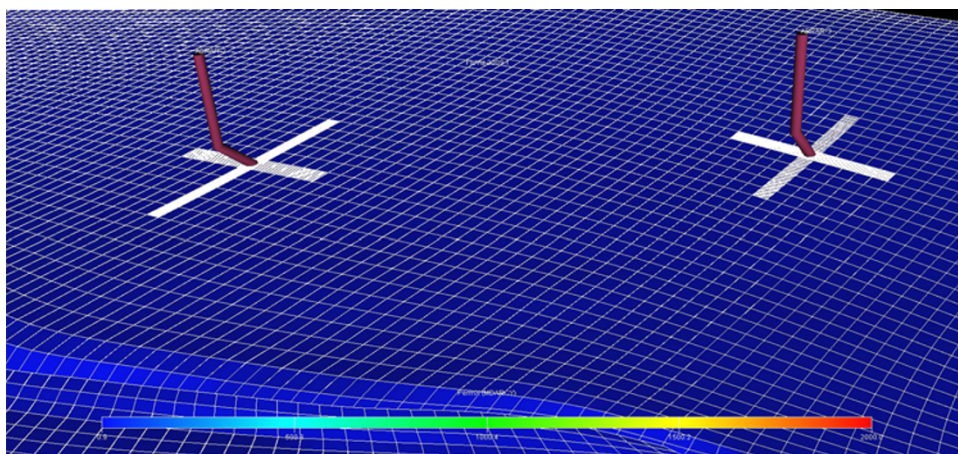**Fig. 3** LGRs around the wellbore

Fig. 4 LGRs around the wellbore

been reviewed in the field study. The interpretation of the well logs shows hydrocarbon bearing in middle A/R G formation which is subdivided into two sand bodies. The two sand bodies were perforated and tested; they showed production with initial rate 370 BOPD by N_2 lifting with traces of water and gas production. Production started from well A-1 (Appendix 1, Fig 16) with ESP yielding a production rate of 350 BOPD and 35 % water cut, then the well production rapidly declined to 130 BOPD and water rate started to decline. The ESP then failed several times and has been replaced with sucker rod pump. The last static fluid level measurement showed average static reservoir pressure of 1,247 psig at a reference depth of −5,300 ft TVDSS. No PVT samples were taken from this field, so calculations were done using both correlations and PVT samples taken from the nearby producing fields. An estimation of the oil in place was done using both material balance and volumetric, showing reserves ranging from 10 to 15 mm STB. Only compression velocity was available from the sonic log and the shear velocity was calculated using the following correlations for both the sand and shale

layers. A static model was built using the available data with approximate cell dimensions of 50 × 50 m and a dynamic model was successively prepared to be used to test the different fracture scenarios (Fig. 2).

The basic simulation model is a three-phase flow single-well model; however, only the oil and gas phase are mobile. The water is not moving as noticed from the well history data, and the amount of produced water at early production period was coming from the water that had been used as a completion fluid, so there is essentially no water production from the well.

Sensitivity runs are completed to determine if grid block size has any impact on the production rates and consequently the fracture length. Static and dynamic models were constructed for this case study; the dynamic model has grid size of 50 × 50 m, consisting of 72,240 cells (80 × 43 × 21). The model is divided into vertical layers. These layers contain productive zones that are fractured and non-productive shale that separate the productive zones. Porosity and permeability for the producing layer is based on the typical values observed in Table 1.

Table 2 Length of LGRs used in the model

			13						
			12						
			11						
			10						
9	*8*	*7*	*6*	Well Cell	*2*	*3*	*4*	*5*	
			14						
			15						
			16						

Cell	Number of divisons	
	x	*y*
Well	17	17
10,11,12	4	17
13	6	17
14,15,16	4	17
6,7,8	17	3
2,3,4	17	3

Each cell has length = 145 feet

Each cell has length = 145 ft
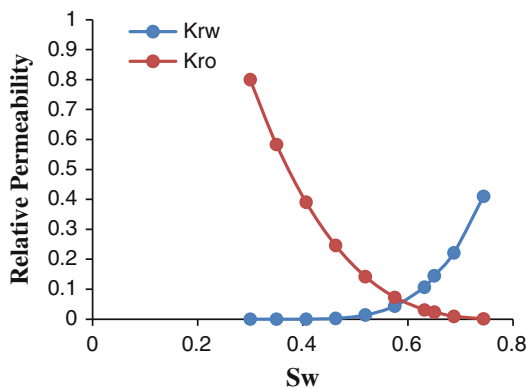
Fig. 5 Relative permeabilities curve

Table 3 PVT and rock data of the studied field

Rock properties		
Compressibility	9.811 E-7 @ 2508 psi	Psi^{-1}
Fluid properties		
Solution gas oil ratio (R_s)	0.03	Mscf/STB
Bubble point pressure	233	Psi
Water formation volume factor	1.01913	rb/stb
Oil density	52.373	Ib/ft^3

39 LGRs were used to model the hydraulic fracture scenarios in three wells; well A-1 (Appendix 1, Fig 16, current well) and the two proposed wells A-2 (Appendix 1, Fig. 17) and A-3 (Appendix 1, Fig. 18). The LGRs were amalgamated in three groups each at the location of each well and were designed so as to match the actual geometry predicted from the rock model as previously mentioned. The original grids were refined depends on the selected length of the fracture to be used in the simulation model. Six grids with size ~145 ft were refined in all directions around the well as Fig. 3 shows; four of them have been refined regularly and the other cells were refined only in one direction depending on the fracture length. For example, the fracture length used in the current model is 600 ft, so represent this length in grid cells with very small fracture aperture; the grid cells should be refined according to that length. Four grid cells of 145 ft+ the rest of the fracture length from the fifth cell around the wellbore, it gives the desired fracture length with its aperture.

By using permeability multiplayer keyword only for the fracture, the hydraulic conductivity value of the created fracture increased as shown in Fig. 3. The red line represents the simulated fracture. Coupling of these LGRs was done by amalgam technique. Simulation of hydraulic fracture using this method resulted in decreasing the convergence and stability issue during the running process; also it gave accurate results. 39 LGRs have been distributed around the main well (1) and the other proposed wells in four directions around the wellbore. Figure 4 shows how the LGRs distributed on the other wells. Table 2 shows some of the LGRs lengths used in the simulation model for the main well.

The PVT data were taken from the nearby operating fields and reservoir properties were populated based on the understanding of the depositional environment to match the
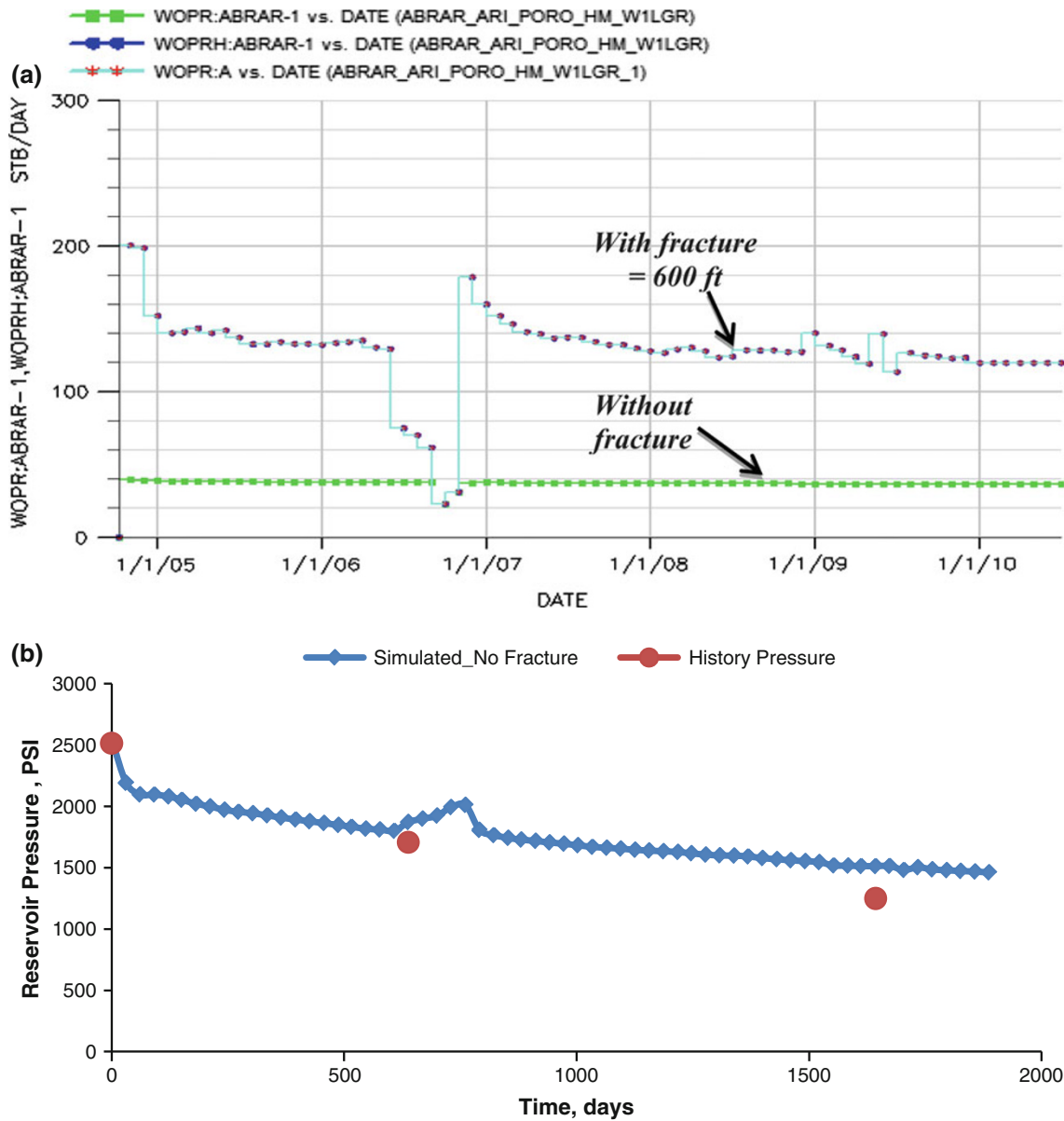
Fig. 6 **a** Relative permeabilities curve. **b** Reservoir pressure matching

existing two wells. The model showed a good match with the original production and pressure data. Table 2 and Fig. 5 show the fluid and SCAL data for the current field (Table 3).

Rock mechanics properties of the simulation model

The model presented here is to simulate a poroelastic reservoir which is intercepted by a vertical wellbore. The reservoir is horizontal and the Cartesian coordinates of the reservoir are aligned in the same direction of minimum and maximum horizontal in situ stresses.

- *Formation properties* Formation rock properties such as Young's modulus, Poisson's ratio, Biot's coefficient, rock strength are assumed to stay constant throughout the simulation time.

Field case study: results

Determining the fracture length

The simulated model is matched to available history data. First the model is run with no fracture. Then an observation
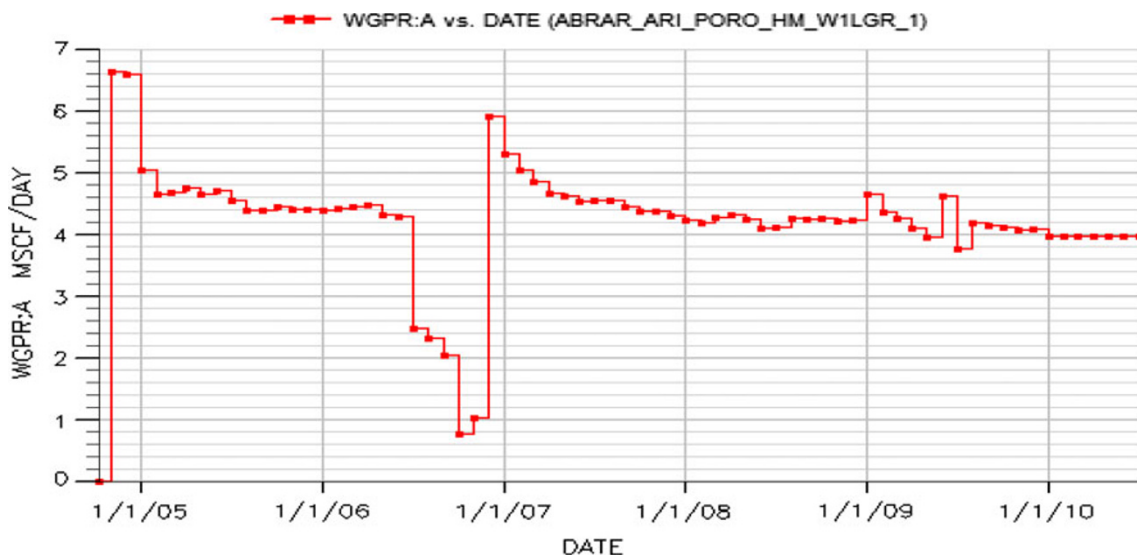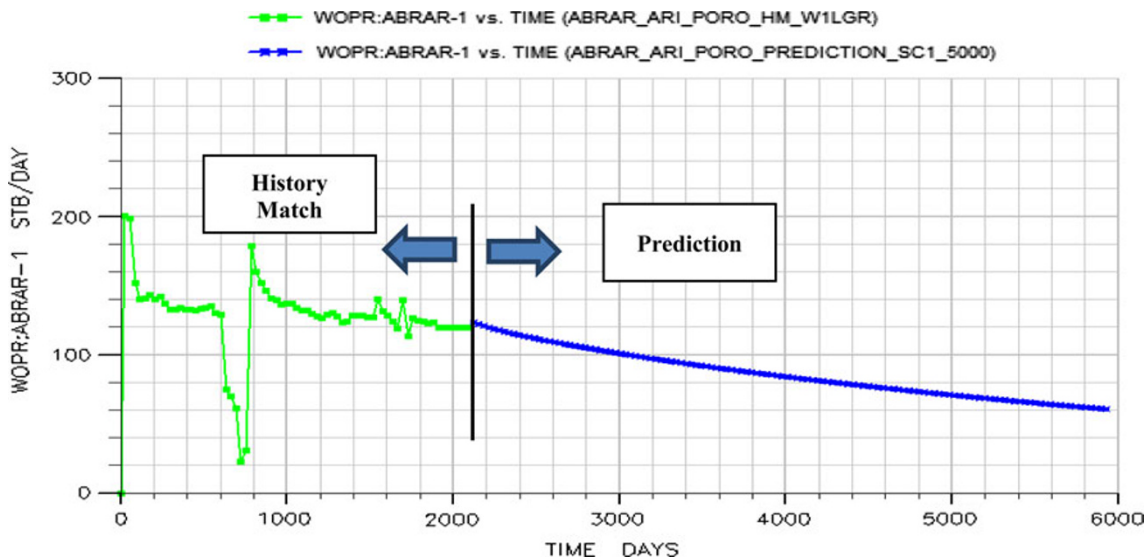
Fig. 7 Gas producing rates

Fig. 8 Prediction of oil rates

has been taken to the matching process. If the production from this model is greater than the measured production, then an adjustment for the porosity and permeability is applied on the grid block according to the petrophysical data to achieve the matching process, and there is no need for running the model with hydraulic fracture scenario. If it does not happen, then the model with initial fracture length is run, and finally the fracture length is changed to match the measured production rates.

Because the permeability of the studied field is very low, changing the friction factor does not significantly change the production rates. When the fracture permeability is increased, it does not result in increase of the flow rates.

This is because the fracture acts like infinite conductivity fracture. History-matching process of the producing well generates fracture length of ∼600 ft. Porosity and permeability values are not changed and stay close to the range of the data measured for the well. The result of history match of the well is shown in Fig. 6a. The line with the lowest production is the run was no fracture includes in the model. Figure 6b shows how the simulated reservoir pressure matched with the observed one.

Although the observed data do not have any recording for the produced gas rates, the model was able to give a trend of the produced gas during the history-matching process by using the solution gas oil ratio (R_s), as Fig. 7 shows.
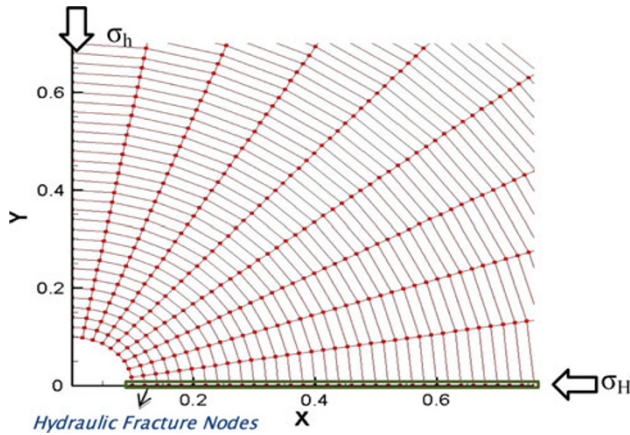
Fig. 9 Mesh used in finite element method

Future production rate

The actual production data and model results are from October 2004 to December 2009. In this section, the simulator is run longer. The simulated production rate curves are extended from December 2009 to December 2019. The simulated values are compared to the actual values between October 2004 and December 2009. This period gives an indication of how good the history-matched model can predict production. The extended simulated rates in the period mentions are found in Fig. 8.

Comparsion the LGRs method with finite element method

A fully poroelastic model is developed to simulate the rock deformation and fluid flow in a reservoir. The governing equations of poroelasticity are solved simultaneously to give change in stress and pressure in the reservoir and it is related to rock deformation by assuming rock to be linearly elastic. The governing equations that guide fluid flow occurring between the reservoir rock and the wellbore are developed from diffusivity equation. These governing equations, which are derived on the basis of mass

continuity equations (for both fluids and solids), Darcy law and equation of equilibrium of solids, are as follows (Charlez 1997: Chen et al. 1995).

$$\phi c_t p - \alpha(\nabla \cdot u) = \nabla \cdot \left(\frac{k}{\mu} \cdot \nabla p\right) + c_f \nabla \cdot p \left(\frac{k}{\mu} \cdot \nabla p\right) \quad (1)$$

$$\left(K + \frac{G}{3}\right) \nabla(\nabla \cdot u) + G\nabla^2 u - \alpha\nabla p \quad (2)$$

where ϕ is the porosity; c_t is the total compressibility; p is the pore pressure; α is the Biot's coefficient; u is the displacement vector; k is the permeability tensor; μ is the fluid viscosity; c_f is the fluid compressibility; ∇ is a vector operator; K is the bulk modulus and G is the shear modulus.

Discretizing the governing equations of poroelasticity by using the finite element method (FEM) (Zienkiewicz and Taylor 2000) results in the following coupled linear systems of equations:

$$\begin{bmatrix} k & Q^T \\ -Q & L + \Delta tH \end{bmatrix} \begin{bmatrix} \Delta u \\ \Delta p \end{bmatrix} = \begin{bmatrix} f_1 \\ f_2 \end{bmatrix} \quad (3)$$

Model geometry includes wellbore, reservoir and two pairs of finite conductive hydraulic fractures (see Fig. 9).The initial maximum and minimum horizontal stresses are along x, y axes, respectively.

There are some assumptions made for finite element model to evaluate the oil production and all of them are as follows:

- The fracture height is equal to the pay zone thickness.
- The reservoir is single-phase state.
- The reservoir is volumetric, i.e., there is neither water encroachment nor water production from the reservoir.
- Isothermal condition.
- Production is assumed to be solely due to change in volume of fluid and rock.

Hydraulic fracture nodes were used to simulate the length, aperture and the conductivity of the existing fracture. The poroelastic model is verified against analytical solutions (Detournay and Cheng 1988) and then it has been

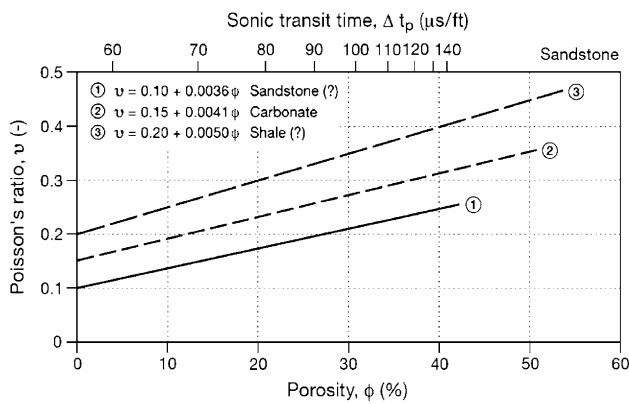**Fig. 10** Prediction of oil rates from two different methods
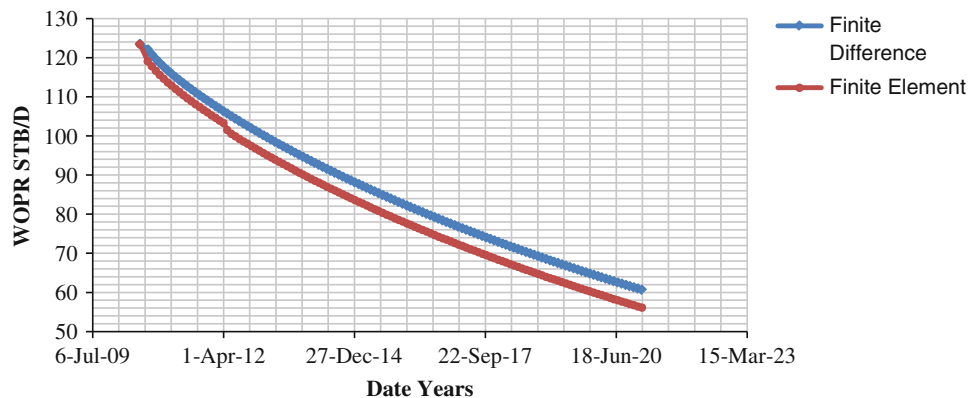
Fig. 11 The relationship between porosity, sonic transit time and Poisson's ratio

Table 4 The rock mechanics calculations

Layer	Top depth (Ft)	Young's modules (Mpsi)	Poisson's Ratio using the chart (FRAC)	Poisson's Ratio using the sonic log (FRAC)
Shale	6050	1.374	0.38	0.38
Sand	6141	2.099	0.205	0.34
Shale	6147.5	2.111	0.355	0.36
Sand	6154.5	2.306	0.2	0.34
Shale	6167	1.693	0.38	0.37
Carbonate	6212.5	7.252	0.19	0.35

extended to predict the oil production rates from 2009 to 2020 for the studied field.

Figure 10 shows the comparison between the oil production rates from the finite difference and finite element method. The matching between the results from the two different methods is good, which is an indication that LGRs method was succeeded in simulating the hydraulic fracture.

Fracture design

In this section, we discussed building the rock mechanics model to design the fracture and how to optimize the fracture design.

Building the rock mechanic model

The rock mechanic properties have been calculated using the open hole logs (sonic, density and neutron porosity logs). Although only compression velocity is available from the sonic log, the shear velocity has been calculated using the following correlations for both the sand and shale layers.

Shear velocity prediction Results from this limited depth range study show that shear velocities vary linearly with compressional velocities for both sands and shale. A linear relationship between V_p and V_s has also been observed by

Castagna et al. (1985) and Williams (1990). The equations for sand and shale shear velocity predictions are given by

$$V_s = 0.7149V_p - 2367.1, \quad \text{Sand}$$
$$V_s = 0.6522V_p - 1902.2, \quad \text{Shale}$$

The rock mechanic properties (Poisson's ratio and Young's modulus) have been calculated using the following correlations:

$$vd = \frac{[(\Delta t_s/\Delta t_c)^2/2 - 1]}{[(\Delta t_s/\Delta t_c)^2 - 1]}$$

$$E_d = \frac{(\rho_b/\Delta t_c)^2[3 - 4(\Delta t_c/\Delta t_s)^2]}{[(\Delta t_s/\Delta t_s)^2 - 1]}$$

The closure pressure for M AR/G and the stress profile for the layers have been calculated using the following correlation:

$$\sigma_2 = \sigma_3 = \frac{v}{1-v}(\sigma_1 - p_f) + p_f$$

The fracture toughness has been calculated using the following correlation

$$K_{IC} = 0.313 + 0.027 * E$$

Another method for calculating the Poisson's ratio has been used, using Fig. 11 which shows the relationship between porosity, sonic transit time and Poisson's ratio. This method is considered less accurate compared with the method discussed above.

Table 4 shows the summary of the rock mechanics calculations for the M AR/G and the layers above and below it. This table also shows good alignment between the calculated Poisson's ratio using the sonic data and the porosity charts for the Shale layers but for the sand layer there is large difference. In order to cover these uncertainties around the Poisson's ratio, different scenarios were used in the stress profile calculations. Appendix 1 presents the different stress profile scenarios.

Optimize the fracture design and pump schedule

Several hydraulic fracture designs were evaluated to determine the optimum fracture design given the uncertainty of the stress profile when compared to the simulation results. Appendix 2 summarizes the results of the different designs comparison.

After this sensitivity analysis we found that massive hydraulic fracturing treatment is required for Fig 16 in order to achieve long half-length and high fracture conductivity. This massive frac will increase the history production rate by 4–5 times. The fracture half-length that could be achieved using the proposed design length ranging between, 600 and 800 ft. The fracture conductivity achieved by using the proposed model, ranging between 10,000 and 20,000 ft (md)
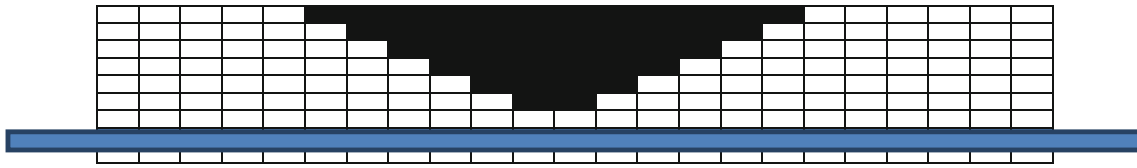
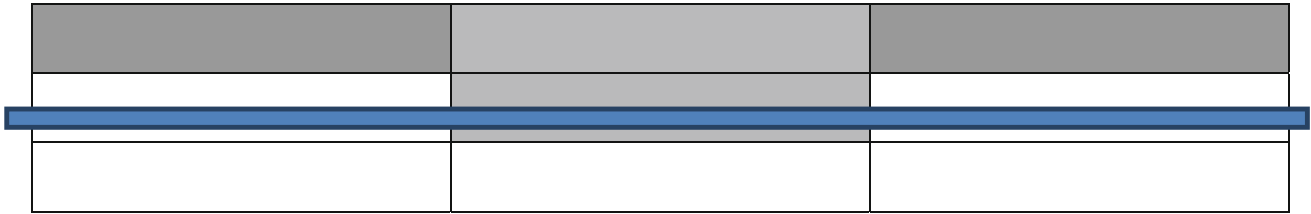**Fig. 12** Gas cone near a horizontal well, fine grid

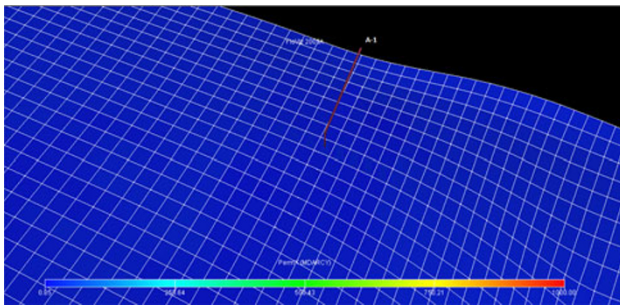**Fig. 13** Gas cone near a horizontal well, coarse grid
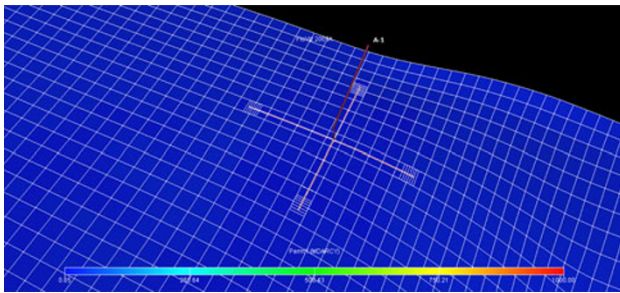

Fig. 14 The dynamic without LGR

Fig. 15 The dynamic with LGR

depends on the proppant type used. Coarse proppant type is preferred (12–18); medium strength will give high conductivity. The amount of proppant required to achieve this design is $\sim$360,000 Lb. In most of the cases the frac height will propagate downward toward the carbonate layer. In order to avoid propagating the frac toward the carbonate layer, very small frac design should be used ($\sim$40,000 Lb of proppant). This small frac size will not increase the productivity from well as required and the production rate is expected to drop rapidly after the fracture. Proppant flow pack additive should be used to avoid proppant flow back after the treatment and avoid damaging the sucker rod pump.

LGR concept and design

In many problems we need a higher resolution (finer grid) than our grid permits. An example is where we model gas coning near the horizontal well. With a high resolution as in Fig. 12, we can track the gas front accurately, and give a good estimate for time and position of the gas breakthrough in the well. Also, the cells are sufficiently small that they can be classified as either gas or oil filled.

When the same problem is modeled on a coarse grid, we see that the shape of the cone is completely lost, and the front is no longer clearly defined (Fig. 13).

Using the resolution of Fig. 12 on the entire grid is typically not possible due to memory limitations and computing time. One possibility is to extend the fine grid in all directions with coarser cells, as shown in Fig. 12. This is, however, not recommended solution, since the resulting long and narrow cells are sources of computational errors, especially when the size difference between large and small cells in the grid becomes too large.

In such situations it is much better to use local grid refinement (LGR). As the name implies, this means that part of the existing grid is replaced by a finer one, and that the replacement is done locally.

The LGRs which will be discussed in this section are regular Cartesian. The appropriate keyword is then CARFIN (Cartesian refinement). Basically a box in the grid is replaced by another box with more cells. The keyword is followed by one line of data, terminated by a slash. Note that only one LGR can be defined in one CARFIN keyword. The keyword must be repeated for each new LGR. Keyword ENDFIN terminates current CARFIN. The syntax is then,

CARFIN

–

– Cartesian Local Grid Refinement

–

– 'Name' I1 I2 J1 J2 K1 K2 NX NY NZ NWMAX Name_of_parent_LGR/

ENDFIN

If we want an LGR on a volume that is not a regular BOX, this can be done by amalgamating several local grids into one. Each of the LGRs must be defined in the standard manner, and hence be on a regular BOX. There is no limit to the number of LGRs that can be amalgamated.

The LGR is the process of dividing one or several grids in the reservoir model into smaller sized grids allowing enhanced grid definition, which is essential for modeling hydraulic fractures using permeability multipliers. Because the fracture does not have a perfect rectangular shape, in fact it usually takes an elliptical shape; it is required to give different ratios in the refinement of each layer which cannot be achieved using only one LGR. This limitation leaves you with the choice of either to use amalgamated LGRs or to choose simplicity and sacrifice modeling the actual geometry; instead you will need to use a rectangular shaped fracture which does not accurately mimic the actual fracture geometry.

In this model several LGRs were needed in order to accurately describe the fracture geometry. LGRs were used for each well, one for every layer. Each layer was divided separately with different ratios to allow sensitivity on the fracture length and height.

This LGR resulted in increase of the grid cells number to be 77,076 cells, which is greater than the original number of cells by 4,836 cells (6.7 %). This increase in the cell number resulted in longer computing time by about 30 % simulated on the same machine which is actually an achievement compared to the normal cartesian LGR; a normal LGR would have increased the number of cells to 116,856 cells (61.8 %) increasing the computing time by up to more than five times the original computing time, and the model required a more powerful workstation to simulate the results (Fig. 14).

The hydraulic fracture is implemented in this simulation study by choosing different cells inside LGR region and multiply its original permeability by a factor in order to represent the hydraulic conductivity of the created fracture as Fig. 15.

The actual field production history was received after the implementation of the optimum frac scenario and was compared to the simulated results to show a match with great accuracy with the predicted rates and pressures. This match validates that the technique used in modeling this frac actually is capable of mimicking the real reservoir performance.

The keywords used in this process were:

LGR It is the first keyword used in the LGR creation, found in the Runspec section, this keyword is used to introduce the number of LGRs present and their main specifications.

CARFIN It is presented in the grid section, and it defines the cells included in the LGR and the number of their subdivisions.

HXFIN &HYFIN It is the keyword responsible for defining the ratios by which the cell should be divided; if not included the cell will be divided equally. This is keyword should be included in the *CARFIN* keyword (i.e., Before *ENDFIN*)

AMALGAM It is the keyword responsible for combining the separate LGRs in one group. Without this keyword LGR cannot be introduced in two adjacent cells.

WELSPECL Used instead of *WELSPEC* keyword for the wells located in the LGR, it used to introduce the wells that are present in the LGR cells.

COMPDATL Used instead of *COMPDAT* keyword for the wells located in the LGR, it is used to introduce the information about the completion for the wells included in the LGR cells.

Conclusion

- Most of the previous publications simulate the hydraulic fracture in a finite difference simulator by using the ordinary technique of grids refinement. The resulting long and narrow cells lead to huge computing errors. This paper presents the concept of LGRs method and its implementation in a finite difference simulator.

- The modeling of hydraulic fractures could be achieved using amalgam LGR as previously shown with small effect on the computing times and will yield reliable and accurate results as concluded from the comparison of the postfrac production to the simulated rates.

- Hydraulic fracturing stimulation is expected to increase the production rate from Abrar-1 well by 2.5–3 times.

- Long half-length (above 600 ft) and high fracture conductivity (above 10,000 ft MD) are required and can be achieved in order to maximize the production rate and ultimate recovery from the reservoir.

- Massive hydraulic fracturing treatment will be required in order to achieve the required objective.

The key risks associated with the fracture treatment are the propagation of the fracture toward the carbonate interval below M.AR/G reservoir. Bending on the permeability of this carbonate layer, water production may be seen after the frac treatment.

Appendix 1: The different stress profile scenarios

See Figs. 16, 17, 18, 19.
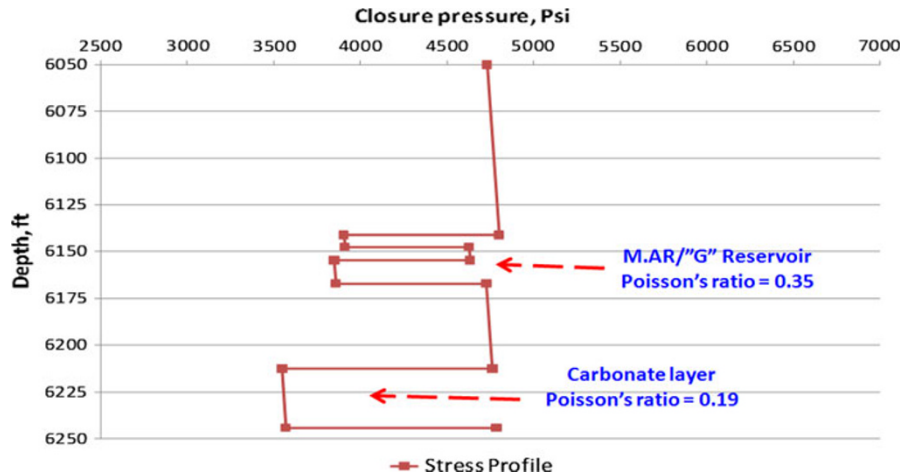

Fig. 16 Stress profile scenario # 1 (base case)
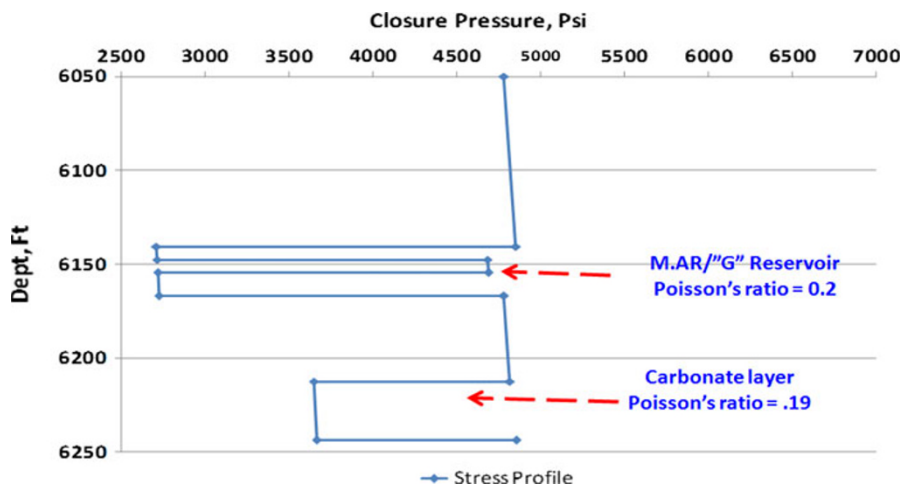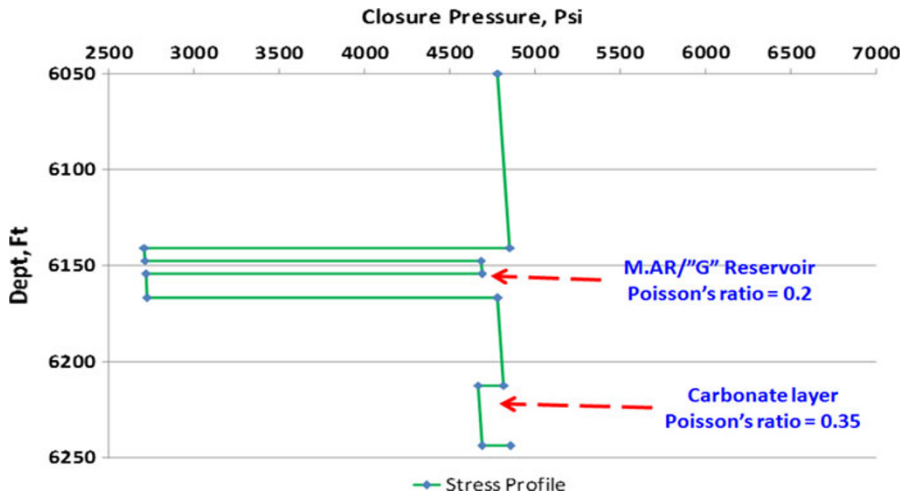

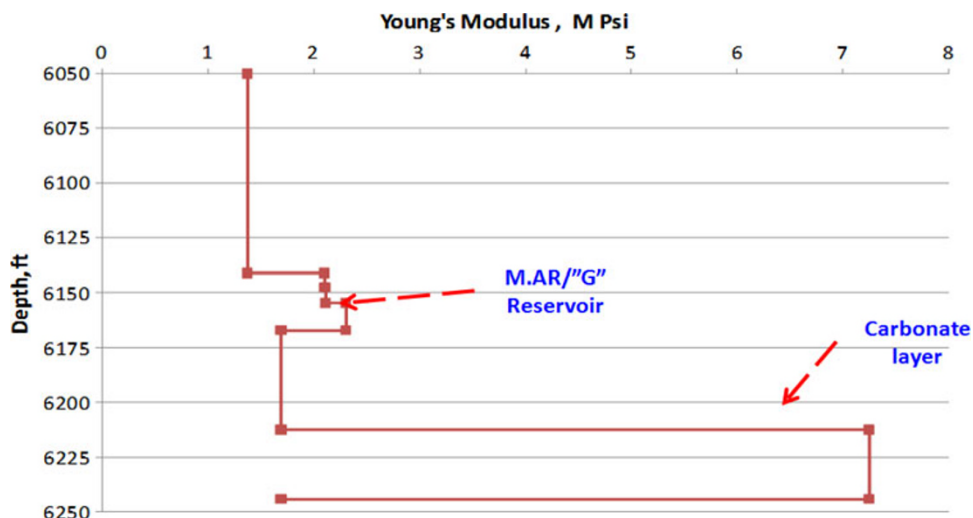Fig. 17 Stress profile scenario # 2

Fig. 18 Stress profile scenario # 3

Fig. 19 Young's modulus profile
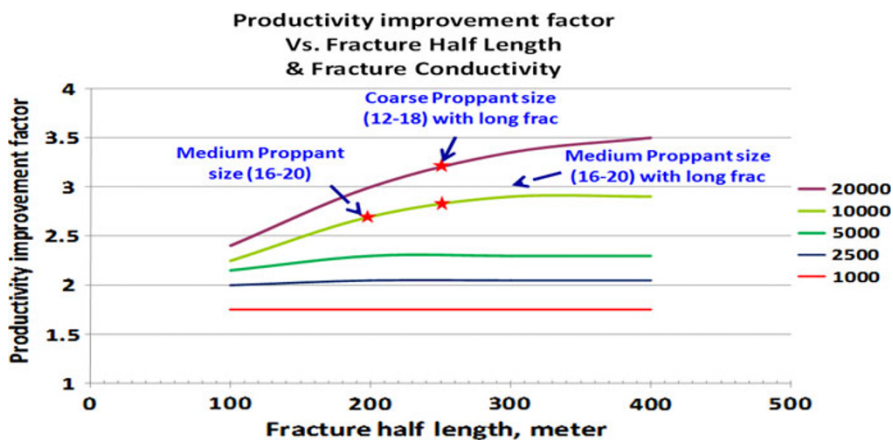
Appendix 2

See Figs. 20, 21, 22, 23.
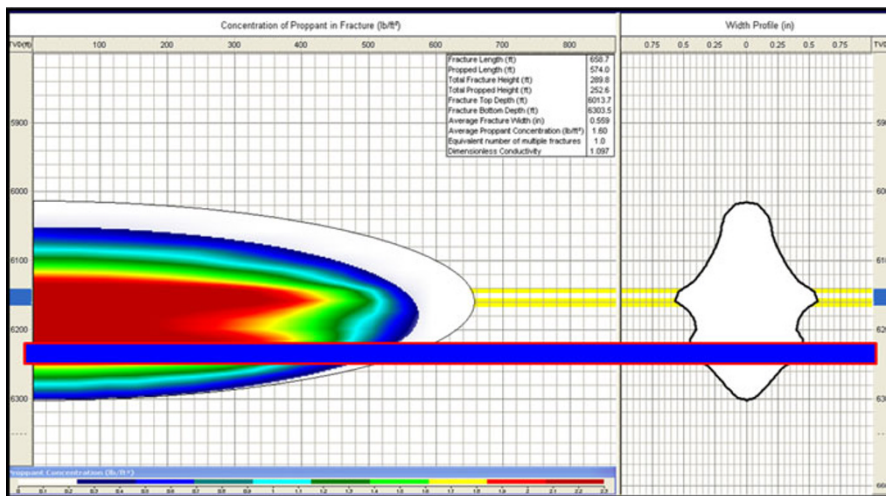

Fig. 20 Frac design optimization

Fig. 21 Fracture profile assuming rock mechanic model scenario # 1 (base case) and medium proppant size (16–20)
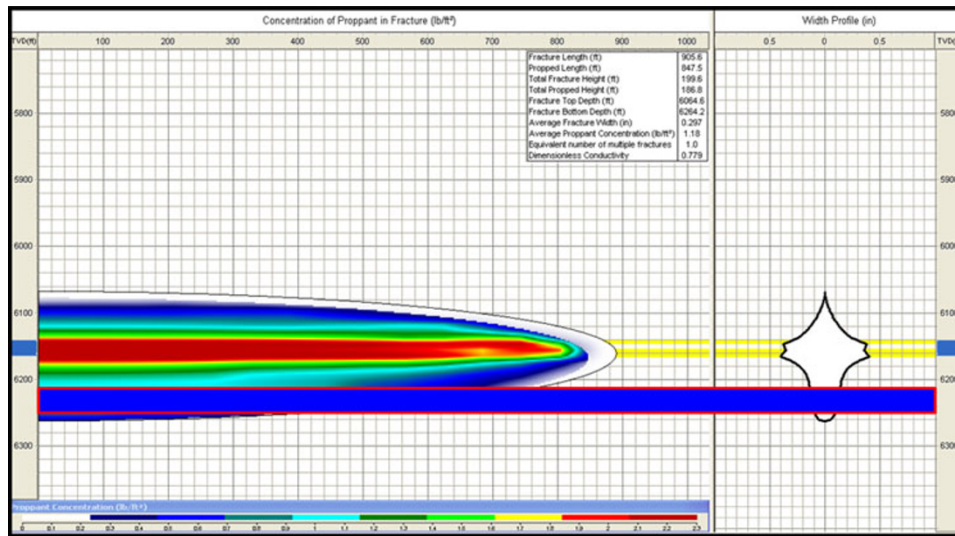
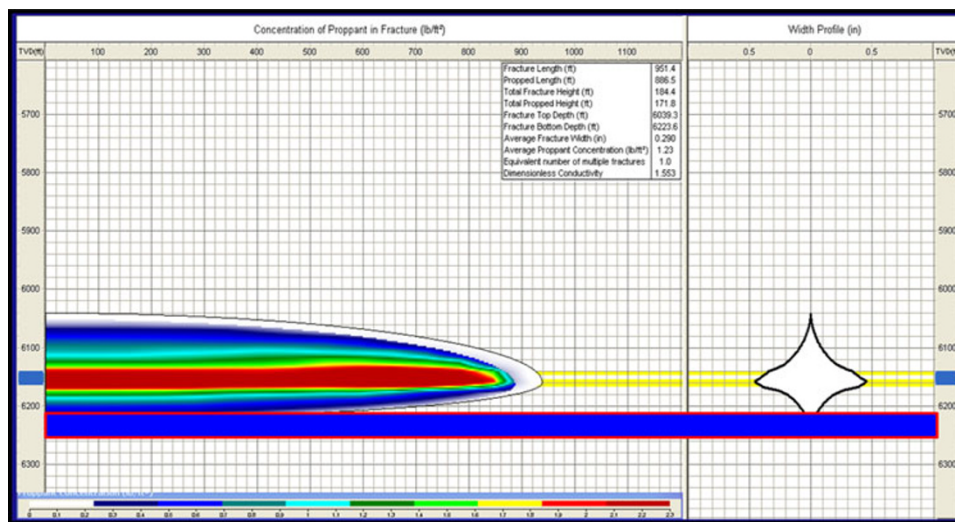**Fig. 22** Fracture profile assuming rock mechanic model scenario # 2 and medium proppant size (16–20)

Fig. 23 Fracture profile assuming rock mechanic model scenario # 3 and medium proppant size (16–20)

Appendix 3

Matrices and vectors involved in Eq. (3) are defined as follows:

$$k = \oint BB^T D d\Omega$$

$$Q^e = \alpha \oint Np^T \left(\frac{\partial Nu}{\partial x} + \frac{\partial Nu}{\partial y} \right) d\Omega$$

$$L^e = \oint \left(ct^i \varphi^{ei} Np^T Np^T \right) d\Omega$$

$$H^e = \oint \frac{k_x}{\mu} \frac{\partial Np^T}{\partial x} \frac{\partial Nu}{\partial x} + \frac{k_x}{\mu} \frac{\partial Np^T}{\partial y} \frac{\partial Nu}{\partial y}$$

$$f_1 = -\Delta t H P$$

$$f_2 = \oint \left(N_u M^T \Delta\sigma \right) d\Gamma$$

In which Ω is the domain and N_p, N_u are pressure and displacement shape functions, respectively, and can be defined as follows:

$$\mathbf{N}_p^T = \begin{pmatrix} N_1 & N_2 \dots N_n \end{pmatrix}$$

$$\mathbf{N}_u^T = \begin{bmatrix} N_1 & 0 & N_2 \dots 0 \\ 0 & N_1 & 0 \dots N_n \end{bmatrix}$$

Also, Γ is the boundary, σ is the stress tensor and:

$$M^T = \begin{bmatrix} n_x & 0 & n_y \\ 0 & n_y & n_x \end{bmatrix}$$

where n_x, n_y are the x, y components of unit normal vector to the boundary.

References

Castagna JP, Batzle ML, Eastwood RL (1985) Relationships between compressional wave and shear-wave velocities in clastic silicate rocks. Geophysics 50:571–581

Charlez PA (1997) Rock mechanics—petroleum application, 2nd edn. Technip, Paris

Chen HY, Teufel LW, Lee RL (1995) Coupled fluid flow and geomechanics in reservoir study—I. Theory and governing equations. Proceeding of the SPE annual technical conference and exhibition, Dallas, Texas, pp 507–519

Detournay E, Cheng AHD (1988) Poroelastic response of a borehole in a nonhydrostatic stress field. Int J Rock Mech Min Sci Geomech Abstract 25(3):171–182

Gidley J et al (1989) Recent advances in hydraulic fracturing, SPE Monograph 12, Richardson, Texas, pp 62–63

Salz LB (1977) Relationship between fracture propagation pressure and pore pressure. Paper SPE 6870 presented at the SPE annual technical conference and exhibition, Denver, Oct. 7–12

Williams DM (1990) The acoustic log hydrocarbon indicator. 31st Annual Logging Symposium, Society of Professional Well Log Analysts

Zienkiewicz OC, Taylor RL (2000) The finite element method — basic formulation and linear problems 1. Butterworth-Heinemann, Oxford